Supplementary information

The optofluidic light cage – on-chip integrated spectroscopy using an anti-resonance hollow core waveguide

Jisoo Kim[a,b], Bumjoon Jang[a,b], Julian Gargiulo[c], Johannes Bürger[d], Jiangbo Zhao[a], Swaathi Upendar [e], Thomas Weiss [e], Stefan A. Maier [c,d], Markus A. Schmidt [a,b,f,*]

a Leibniz Institute of Photonic Technology, Albert-Einstein-Str. 9, 07745 Jena, Germany

b Abbe Center of Photonics and Faculty of Physics, Friedrich-Schiller-University Jena, 07743 Jena, Germany

c The Blackett Laboratory, Department of Physics, Imperial College London, London SW7 2AZ, United Kingdom

d Chair in Hybrid Nanosystems, Ludwig-Maximilians-Universitat Munich, 80799 Munich, Germany

e 4th Physics Institute, University of Stuttgart, Pfaffenwaldring 57, 70569 Stuttgart, Germany

f Otto Schott Institute of Materials Research (OSIM), Friedrich Schiller University Jena, 07743 Jena, Germany

Simulation of the fraction of power inside the strands

The fundamental core mode and fields of the light cage structure described in the main text have been simulated using the multipole expansion method (Cudos MOF). The fields have been normalized using the following normalization condition[1-2]:

$$1 = S_0 + L_0 \tag{1}$$

This condition contains a surface integral over a finite circular cross section of radius r_n:

$$S_0 = \int_0^{2\pi}\int_0^{r_n}\rho(E_\rho H_\varphi - E_\varphi H_\rho)d\rho d\varphi. \tag{2}$$

Furthermore, L_0 is a line integral at the circle with radius r_n:

$$L_0 = \frac{\varepsilon\mu k_0^2 + \beta^2}{2\left(\varepsilon\mu k_0^2 - \beta^2\right)^2}\int_0^{2\pi}\left(E_z\frac{\partial H_z}{\partial\varphi} - H_z\frac{\partial E_z}{\partial\varphi}\right)_{r=r_n} d\varphi + \frac{k_0\beta r_n^2}{2\left(\varepsilon\mu k_0^2 - \beta^2\right)^2}$$
$$\int_0^{2\pi}\left\{\mu\left[\left(\frac{\partial H_z}{\partial\rho}\right)^2 - \rho H_z\frac{\partial}{\partial\rho}\left(\frac{1}{\rho}\frac{\partial H_z}{\partial\rho}\right)\right] + \varepsilon\left[\left(\frac{\partial E_z}{\partial\rho}\right)^2 - \rho E_z\frac{\partial}{\partial\rho}\left(\frac{1}{\rho}\frac{\partial E_z}{\partial\rho}\right)\right]\right\}_{\rho=r_n} d\varphi \tag{3}$$

Here, β is the propagation constant, k_0 is the wavenumber, ε and μ denote the permittivity and the permeability in the cladding region. The electric and magnetic fields are denoted by **E** and **H**, respectively. For these normalized fields, we then calculated the fraction of power within the strands as explained in the main text and as shown in Figure 1(e).

As mentioned in the main text the spike-like feature at around $\lambda = 698\text{nm}$ results from an anti-crossing of the central core mode with one of the strand supermodes. To show this hybrid mode situation more clearly, the spectral distribution of f in the vicinity of that wavelength together with the corresponding Poynting vector distribution is shown in Figure S1.

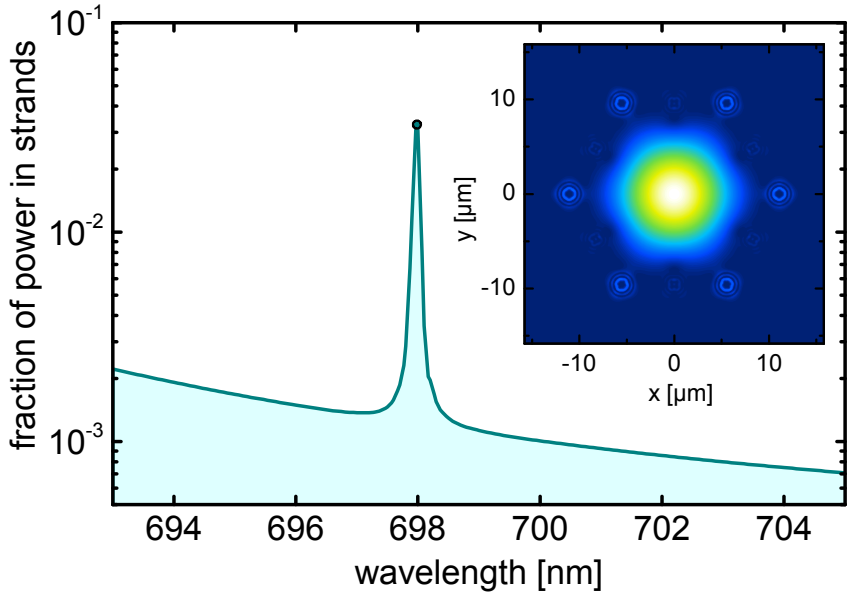

Figure S1: Close-up of the spectral distribution of the fraction of power in the strand in the vicinity of the spike-like feature at $\lambda = 698\text{nm}$ (indicted by the dot). The inset shows the corresponding Poynting vector distribution (color scale ranges linearly from 1 (white) to zero (dark blue)).

Estimation of impact of reinforcement rings on modal attenuation

To analyse the influence of the reinforcement rings on modal losses, the coupling efficiency η_r between the modes of the light cage inside and outside the ring domain at the main absorption line of the dye ($\lambda = 527\text{nm}$) was calculated (Figure S2). This quantity represents the fraction of power lost each time the mode reaches a different section of the light cage. The basis for this estimation forms the usual expression for the coupling efficiency, which includes the electric fields of the two modes involved. Note that the amplitude of the fields outside the domain of the light cage increases as leaky modes are taken into account. Thus, the integration area has been limited to the inside and the nearest surroundings of the light cage cross-section (lateral integration area 30µm × 30µm).

$$\eta_r = \frac{|\int E_1 \cdot E_2 dA|^2}{\int |E_1|^2 dA \cdot \int |E_2|^2 dA} \qquad (4)$$

Due to the pronounced similarity of the two modes (Figure S2), the coupling efficiency is close to unity ($\eta = 0.997$). Thus the power loss per scattering event is very small and thus the influence of the ring on the optical properties can be safely neglected throughout the entire discussion.

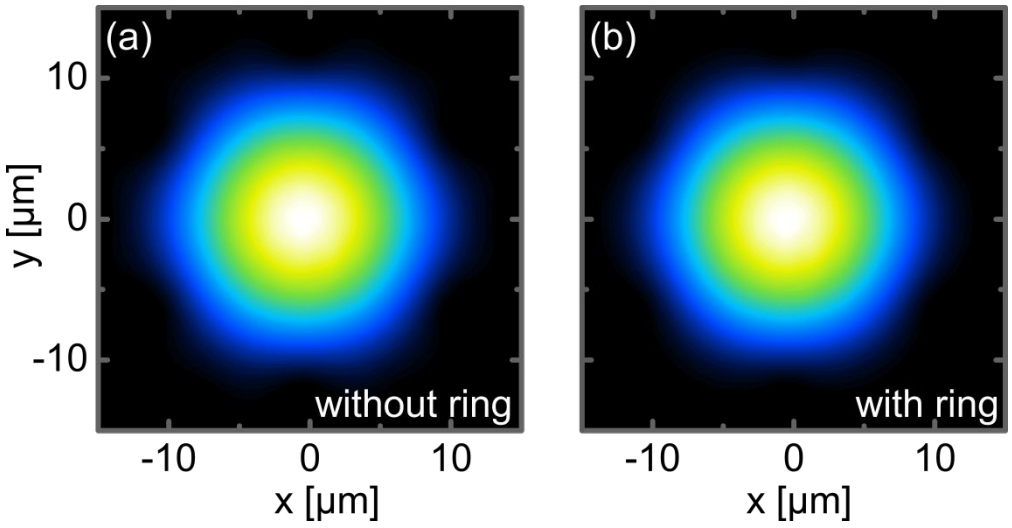

Figure S2: Simulated spatial distributions of the intensity ($\lambda = 527\text{nm}$) of the mode in the light cage in (a) absence and (b) presence of the reinforcement ring.

Dependence of various parameters on pitch

To unlock the dependence of some of the key benchmark figures of the optofluidic light cage on structural variations, the pitch dependence of (i, Figure S3(a)) the imaginary part of the effective index $\text{Im}(n_{eff})$, (ii, Figure S3 (b)) the fraction of field inside the analyte f_a and (iii, Figure S3 (c)) the mode field diameter (MFD) of the fundamental mode of the light cage MFD_{LC} have been calculated (MFD defined in [3]). The simulations were conducted at a wavelength of lowest loss in one transmission band (here λ=0.642 µm, Figure 1(d)). For a comparison to the light cage free situation the mode field diameter of a comparable Gaussian beam $MFD_G = 2w(z) = 2w_0\sqrt{1 + (\lambda z/\pi n w_0^2)^2}$ which has a waist w_0 that is identical to half of the extension of the light cage core ($w_0 = 2\Lambda$) and which freely diffracts across the length of the light cage used in the experiment ($L = 5\text{mm}$, Figure S3(c)) was additionally determined.

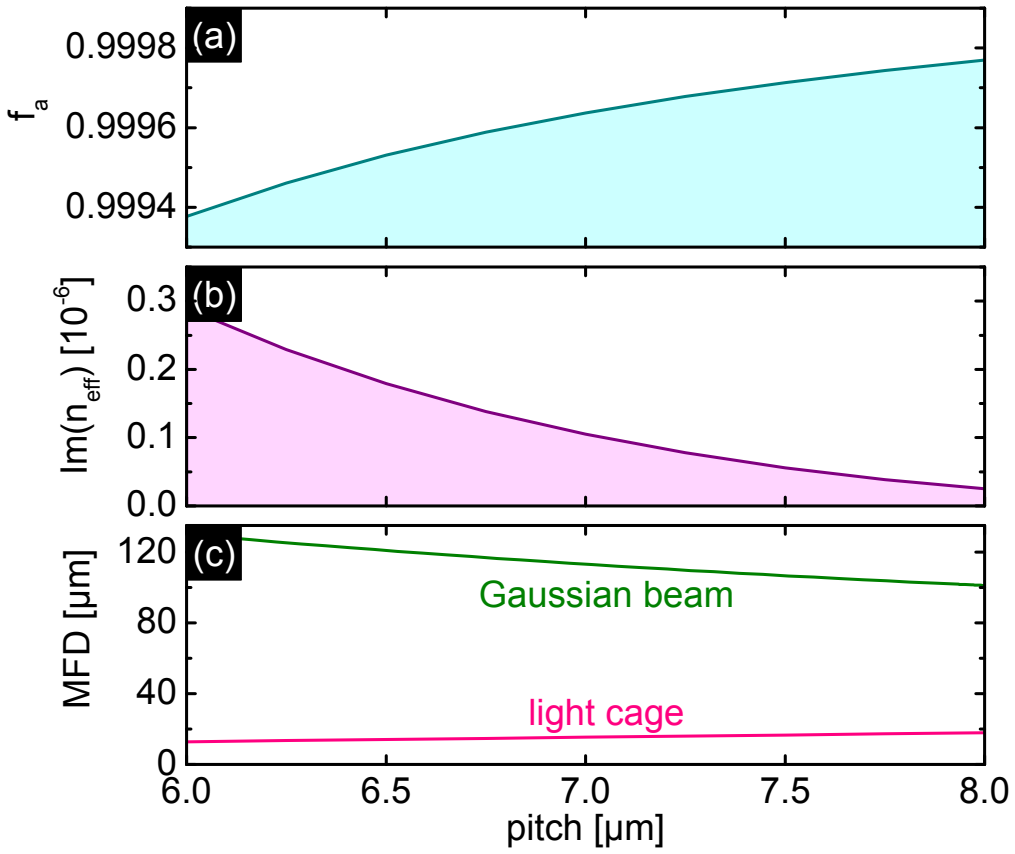

Figure S3: Simulations showing the pitch dependence of (a) the imaginary part of the effective index $\text{Im}(n_{eff})$, (b) the fraction of field inside the analyte f_a and (c) the mode field diameter of the fundamental mode of the light cage MFD_{LC}. The simulations were conducted at a wavelength of lowest loss in one transmission band (here $\lambda = 0.642$ µm). The green curve in (c) refers to a Gaussian beam which freely diffracts across the length of the experimentally investigated light cage ($L = 5\text{mm}$, details in the text).

The results shown in Figure S3 reveal three main points:

1. The fraction of power inside the analyte only weakly depends on Λ and is close to unity for the pitch values considered here ($f_a > 0.994 \approx 1$, Figure S3(a)), showing that the assumption of neglecting the fraction of power in the strands within Lambert-Beer-law ($f \approx 0$) is also valid for other light cage configurations.

2. Increasing Λ imposes modal attenuation to decrease within the same order of magnitude (Figure S3(b)) while MFD_{LC} simultaneously increases (pink curve in Figure S3(c)).
3. For any of the pitch values considered here MFD_{LC} is at least one order of magnitude smaller than MFD_G.

Therefore the optimal choice of geometric parameters depends on the requirements of the application under consideration and on the degree of mode confinement that should be established. It is important to note that for any pitch value considered here the light cage offers diffraction free propagation across millimetre distances within a strongly confined mode in contrast to a diffracting Gaussian beam reaching mode field diameters $> 100\mu m$ for $\Lambda < 8\mu m$.

Implementation

Direct laser writing has been used for the implementation of the light cage structures. Before the actual device fabrication, the surface of the silicon substrate has been silanized to improve its bonding to the polymeric microarchitectures[4]. Cleaning of the silicon chips was conducted via successive ultra-sonication in acetone, IPA and ethanol (15 minutes each) and drying with nitrogen. Subsequently the chips were treated with oxygen plasma (1 minute, 150W) to generate a hydrophilic surface. After that, the treated chips were immersed in a mixture of 3-(trimethoxysilyl)propyl methacrylate (440159 from Sigma-Aldrich, Inc., 300 µL) and ethanol (30 mL) overnight and dried with nitrogen.

The actual implementation of the light cages relies on IP-DIP negative photosensitive resist (Nanoscribe GmbH) and a 63 × objective (1.4 NA, Plan Apochromat from Zeiss) for the focussing of the pulse laser beam in order to precisely construct the light cages on the silicon chips. There are three elements (solid support post, the strands and the reinforcement ring) within one segment (length 180µm) of the light cage. First, solid posts were implemented every 180 µm (cross-section and height: 35 µm × 35 µm and 50 µm) to elevate the light cage from the substrate. The strands and the reinforcement rings were then printed according to a hexagonal array, which consists here of 12 strands (strand diameter d = 3.6 µm) including reinforcement rings for mechanical support (thickness and length: 1 µm and 2 µm) every 30 µm. This reinforcement ring connects adjacent strands thus preventing mechanical collapse of the entire structure during development. The duration for creating one light cage of length of 4.5mm was approximately 1.5 h (writing speed: 55 mm/s). Finally, the printed samples were developed using 30 mL propylene glycol methyl ether acetate (PGMEA, ≥ 99.5%, 484431 from Sigma Aldrich, Inc.) for 20 minutes and 30 mL NovecTM (SHH0002 from Sigma Aldrich, Inc.) for 2 minutes. Finally, the samples were rinsed by distilled water and IPA to remove the uncured photoresist. Further details can be found in our previous work[5].

Liquid solutions

Preparation of water/IPA solutions

For uncovering the dependence of the optical properties of the light cages on the surrounding refractive index four different mixtures of isopropanol (isopropyl alcohol, IPA, ≥ 99.9% Carl Roth GmbH) and distilled water were prepared (IPA/water mass fraction: 0, 20, 44, 55, and 100 wt%). Prior to the optical experiment the refractive index of each solution was measured via refractometry.

Preparation of dye solutions

The dye measurements were carried out using Rhodamine 6G (R6G, R4127 from Sigma-Aldrich, Inc.). A stock solution with high R6G concentration (150 µM) in distilled water has been prepared and deliberately diluted in the fluidic cell. The R6G concentrations used here were 15, 10, 5, 3, 2.5, and 2 µM. All prepared dye solutions have been characterized prior to the light cage experiments using cuvette-based absorption spectroscopy. The absorption spectrum of R6G in water was confirmed by UV-VIS Spectrophotometer (V-660 from JASCO Deutschland GmbH), showing strongest absorption at $\lambda = 527$ nm.

Implementation of liquid chamber

The optofluidic chambers used in this work have been realized by using Polydimethylsiloxane (PDMS, Sylgard 184 from Dow corning). Specifically, 1g of the base resin was mixed with the curing agent (ratio: 10:1) and the

solution was put in an evacuated desiccator for 1h to remove air bubbles. The treated mixture was poured over a negative mould and placed again in vacuum for 30 min. The mould was then baked in an oven at 60 ℃ for 2 h thus to cure the PDMS. After complete curing, the PDMS casting was separated from the negative mould, cleaned in ethanol and dried with nitrogen. The PDMS casting was terminated by glass slides (thickness 0.5mm) on both sides of the casting for optical access finally leading to a total chamber volume of 500 µL. The PDMS casting and glass slides were treated by oxygen plasma (150W) for 30s. Finally, the silicon chips containing the light cages were fixed at the bottom of the fluidic cell using a prepolymer which was mixed with base resin and curing agent in a 2:1 ratio. The fluidic cell including the light cage was then finalized by overnight baking in the oven at 45 ℃. The final fluidic cell (Figure S4) has a width, height, and thickness of 1.5cm, 0.7cm and 0.5cm, respectively.

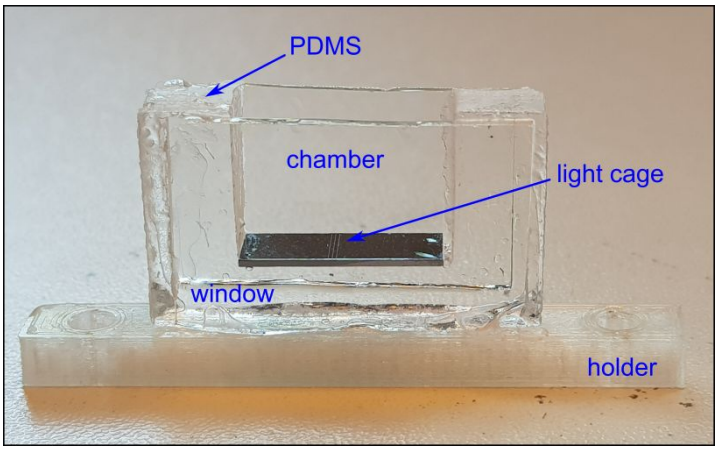

Figure S4: Photo of the liquid cell used for the optical characterization of the optofluidic light cages.

Optical characterization setup

The optical measurements were conducted by a transmission setup (Figure S5) that was composed of a broadband white light source ($450\text{nm} \leq \lambda \leq 2.4\mu\text{m}$, SuperK COMPACT, NKT Photonics), a notch filter to remove residual pump light at 1065nm (Edmund Optics), objectives for in- and outcoupling ($20\times$, 0.50 NA, RMS20X-PF from Olympus Corp.; $10\times$, 0.30 NA, N10X-PF from Nikon Corp.), and coupling stages. An optical spectrum analyser (AQ-6315A from Ando) connected to the multimode fiber (0.22 NA, FG050LGA from Thorlabs, Inc.) was used for spectral characterization, while a CCD camera (DCC1240C from Thorlabs, Inc.) was used to measure the output mode field pattern.

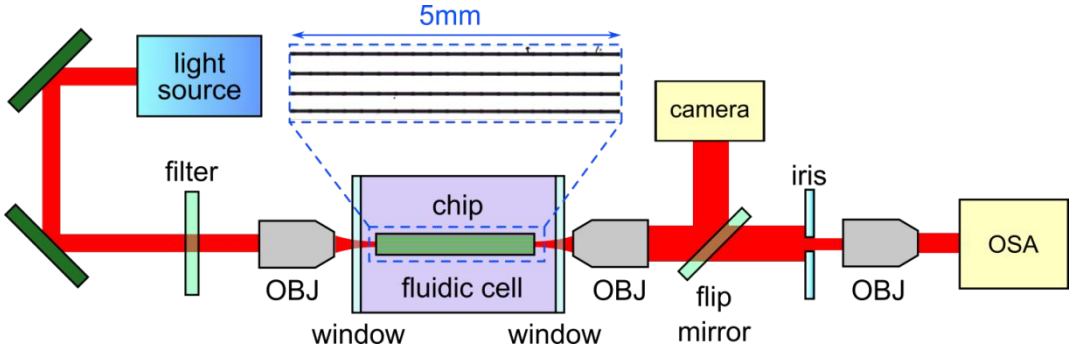

Figure S5: Schematic of the transmission setup used to optically characterize the optofluidic light cages. The image in the centre of the schematic shows a photograph of an example sample (top view) containing four light cages.

Estimation of losses in optofluidic light cage

The modal attenuation at the main absorption line of the dye (here $\lambda = 527\text{nm}$, Figure 3) can be estimated by using Eq. 2 which can be written in the following form

$$A = -\log_{10}(P/P_0) = -\log_{10}(\eta) + \epsilon(1-f)cL + \frac{\alpha L}{10} = b + m \cdot c \qquad (5)$$

and holds for both cuvette and light cage. For the cuvette the entire electromagnetic field is interacting with the liquid ($f = 0$) leading to $A_{cuv} = b_{cuv} + m_{cuv}c$ with b_{cuv} accounting for loss in absence of the dye. In case of the light cage operation in a high transmission band is considered, allowing to consider $f \approx 0$ (Figure 1(e)) and thus leading to $A_{LC} = b_{LC} + m_{LC} \cdot c$. Both dependencies have been measured in the experiments (inset of Figure 3b) showing identical slope parameters $m_{cuv} \approx m_{LC}$ (Tab. 1 of the main text). Taking the difference between the two equations leads to $\Delta b = b_{LC} - b_{cuv} = -\log_{10}(\eta) + \alpha L/10$ which can be straightforwardly solved for the modal attenuation $\alpha = \frac{10}{L}(\Delta b + \log_{10}(\eta))$. The value of Δb can be taken from the experimental data (inset of Figure 3b), which in the present case yields $\Delta b = 0.6690 - 0.1081 \approx 0.5609$. This allows plotting the modal attenuation of the light cage as a function of coupling efficiency which is unknown here (Figure S6).

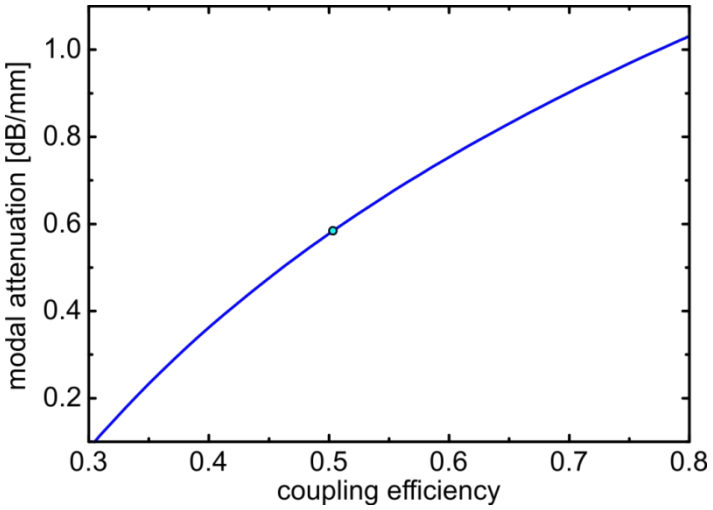

Figure S6: Modal attenuation of the R6G-water filled light at $\lambda = 527\text{nm}$ cage as a function of coupling efficiency obtained using the above procedure. The dot indicates an assumed coupling efficiency of 50%.

Assuming a coupling efficiency of about 50% (dot in Figure S6) losses of the order of 0.58dB/mm are obtained, which is reasonable and represents a values that is in accordance with preliminary measurements of light cages in air [5].

Refractive indices used in simulations

The spectral distribution of the refractive index of the exposed polymer used in the 3D nanoprinting process has been taken from[6] and is given by

$$n_{polymer} = \sqrt{1 + \frac{1.342468 \cdot \lambda^2}{\lambda^2 - 0.128436^2}} \qquad (6)$$

Note the excellent agreement between measured dips in the transmission spectrum and the simulated cut-off wavelengths of the isolated strand mode shown in Figure 2(c) and in[7] confirm the validity of this expression.
For the material dispersion of water the following expression has been used[8]

$$n_{water} = 1.3199 + \frac{6878}{\lambda^2} - \frac{1.132 \cdot 10^9}{\lambda^4} + \frac{1.11 \cdot 10^{14}}{\lambda^6} \qquad (7)$$

Refractive index of the water-IPA mixture

Refractive indices of binary solvent mixtures are given as follow

$$n^2 = \frac{3}{1 - \frac{N_A}{3\varepsilon_0}\left(\frac{c_{H2O}}{M_{H2O}}\alpha_{H2O} + \frac{c_{IPA}}{M_{IPA}}\alpha_{IPA}\right)\rho_{mix}} \qquad (8)$$

where N_A is Avogadro constant, ε_0 vacuum permittivity, $c_{H2O/IPA}$ the mass ratio of the component, $M_{H2O/IPA}$ the molar mass of the solvent, $\alpha_{H2O/IPA}$ the molecular polarizability of the specie, and ρ_{mix} the corresponding density of the mixture, for which the values are from literature[9].

Then, the resonance amplitude ($A(c)$) and wavelength ($\lambda_e(c)$) (shown in Figure S7) of a mixture can be extracted out from fitting one-item Sellmeier equation:

$$n(\lambda,c) = \sqrt{1 + \frac{A(c)\cdot\lambda^2}{\lambda^2 - \lambda_e^2(c)}} \qquad (9)$$

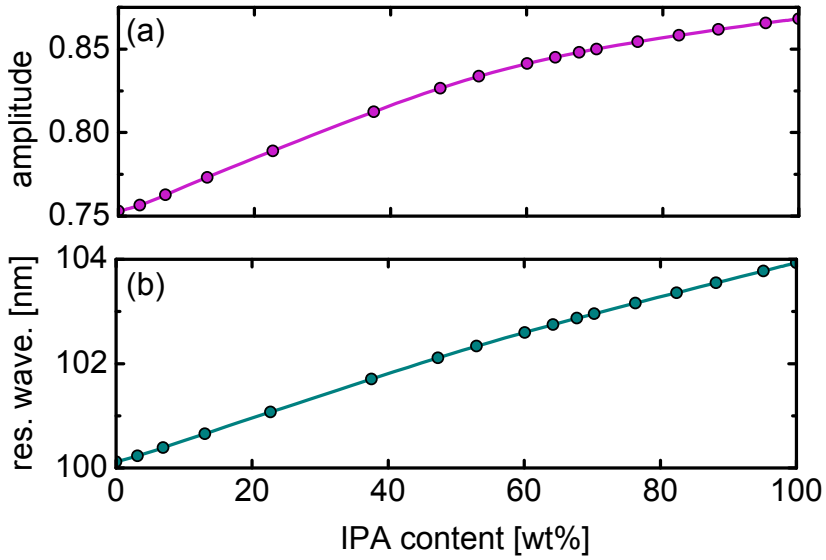

Figure S7: Dependence of amplitude A (a) and electronic resonance wavelength λ_e (b) on IPA concentration.

Cut-off equation is the isolated strand modes

As shown in[7] the spectral positions of the transmission dips can be approximated by the cut-off wavelengths of the isolated modes in the weak guidance approximation. These wavelengths can be found by the following equation[10]:

$$0 = j_{l-1,m} - \frac{d\pi}{\lambda}\sqrt{n_p(\lambda)^2 - n_{liquid}^2(\lambda)} \qquad (10)$$

with the m^{th}-root of the Bessel function j_{m-1}.

Comparison to other works

Table S1: Comparison of reported waveguide systems used for absorption spectroscopy (green: this work, red: slab waveguide, blue: rib-type waveguide, purple: optical fiber). In the most right column, the number indicate the respective work in the reference list of the SI, while the number in brackets refers to the number of the reference list of the main text.

Type of waveguide	device length	Lateral dimension (approx.)	minimal concentration	Limit of detection	spectral domain	Ref.
Light cage	4.5mm	24µm x 24µm	2µM in R6G	0.09µM in R6G	VIS	This work
Slab waveguide	30mm	16.7mm x 10mm	1µM in R6G	N.A	VIS	[11] [51]
Slab waveguide	5mm	20mm x 10mm	2.2µM in R6G	0.01µM in TNT	VIS	[12] [52]
Planar nanoribbon	1.5mm	Diameter= 150nm and 200nm	6µM in R6G	0.3mM in EITC(eosin-5-isothiocyanate)	VIS	[13] [53]
Polymer core	11cm	40µm x 50µm	Unknown	N.A	VIS	[14] [54]

waveguide						
Liquids core fiber	129.5cm	Diameter=1mm	0.13nM inR6G	N.A	VIS	[15] [55]
Hollow core fiber	100cm	Diameter=30μm	0.1μM in SMX	0.05μM in SMX	UV-VIS	[16] [27]

Parameters used in this work

parameter	abbreviation	unit
Power after sample	P	W
Power before sample	P_0	W
Absorbance	A	1
Molar attenuation coefficient (molar absorptivity)	ϵ	$\mathrm{M}^{-1} \cdot \mathrm{cm}^{-1}$
Transmission	T	dB
Coupling efficiency	η	1
Molar concentration	c	mol/L
Modal attenuation	α	cm^{-1}
Slope parameter	m	L/mol
Offset parameter	b	1
Fraction of optical power in the strands	f	1
Standard deviation of absorbance	σ_A	1

REFERENCES

(1) Upendar, S.; Allayarov, I.; Schmidt, M. A.; Weiss, T., Analytical mode normalization and resonant state expansion for bound and leaky modes in optical fibers - an efficient tool to model transverse disorder. *Opt. Exp.* **2018,** *26* (17), 22536-22546.

(2) Allayarov, I.; Upendar, S.; Schmidt, M. A.; Weiss, T., Analytic Mode Normalization for the Kerr Nonlinearity Parameter: Prediction of Nonlinear Gain for Leaky Modes. *Phys Rev Lett* **2018,** *121* (21), 213905.

(3) Koshiba, M.; Saitoh, K., Structural dependence of effective area and mode field diameter for holey fibers. *Opt. Exp.* **2003,** *11* (15), 1746-1756.

(4) Liu, X.; Gu, H.; Wang, M.; Du, X.; Gao, B.; Elbaz, A.; Sun, L.; Liao, J.; Xiao, P.; Gu, Z., 3D Printing of Bioinspired Liquid Superrepellent Structures. *Adv. Mater.* **2018,** *30* (22), 1800103.

(5) Jain, C.; Braun, A.; Gargiulo, J.; Jang, B.; Li, G.; Lehmann, H.; Maier, S. A.; Schmidt, M. A., Hollow Core Light Cage: Trapping Light Behind Bars. *Acs Photonics* **2019,** *6* (3), 649-658.

(6) Jang, B.; Gargiulo, J.; Ando, R. F.; Lauri, A.; Maier, S. A.; Schmidt, M. A., Light guidance in photonic band gap guiding dual-ring light cages implemented by direct laser writing. *Opt. Lett.* **2019,** *44* (16), 4016-4019.

(7) Jang, B.; Gargiulo, J.; Ziegler, M.; Ando, R. F.; Hübner, U.; Maier, S. A.; Schmidt, M. A., Fine-tuning of the optical properties of hollow-core light cages using dielectric nanofilms. *Opt. Lett.* **2020,** *45* (1), 196-199.

(8) Bashkatov, A.; Genina, E., Water refractive index in dependence on temperature and wavelength: A simple approximation. *Proceedings of SPIE - The International Society for Optical Engineering* **2003,** *5068*.

(9) Herráez, J. V.; Belda, R., Refractive Indices, Densities and Excess Molar Volumes of Monoalcohols + Water. *Journal of Solution Chemistry* **2006,** *35* (9), 1315-1328.

(10) Snyder, J. A.; Love, J. D., *Optical waveguide theory*. Chapman and Hall: London ; New York, 1983.

(11) Matsuda, N.; Takatsu, A.; Kato, K., Absorption Spectra of Rhodamine 6G by Slab Optical Waveguide Spectroscopy. *Chem Lett* **1996,** *25* (2), 105-106.

(12) Liu, P.; Li, Z.; Li, B.; Shi, G.; Li, M.; Yu, D.; Liu, J., The analysis of time-resolved optical waveguide absorption spectroscopy based on positive matrix factorization. *J Colloid Interf Sci* **2013,** *403*, 134-141.

(13) Sirbuly, D. J.; Tao, A.; Law, M.; Fan, R.; Yang, P., Multifunctional Nanowire Evanescent Wave Optical Sensors. *Adv. Mater.* **2007,** *19* (1), 61-66.

(14) Jiang, L.; Pau, S., Integrated waveguide with a microfluidic channel in spiral geometry for spectroscopic applications. *Appl. Phys. Lett.* **2007,** *90* (11), 111108.

(15) Krockel, L.; Frosch, T.; Schmidt, M. A., Multiscale spectroscopy using a monolithic liquid core waveguide with laterally attached fiber ports. *Anal Chim Acta* **2015,** *875*, 1-6.
(16) Nissen, M.; Doherty, B.; Hamperl, J.; Kobelke, J.; Weber, K.; Henkel, T.; Schmidt, M., UV Absorption Spectroscopy in Water-Filled Antiresonant Hollow Core Fibers for Pharmaceutical Detection. *Sensors-Basel* **2018,** *18* (2), 478.